Nanoscale Advances

ROYAL SOCIETY OF CHEMISTRY

PAPER

View Article Online
View Journal | View Issue



Cite this: *Nanoscale Adv.*, 2023, **5**, 3934

# *In situ* infrared CO detection using silver loaded EMT zeolite films†

Yuda Wang,‡[a] Haitao He,‡[a] Jiao Sun, *[a] Xinyao Zhang,[a] Mahmut Zulpya,[a] Xianhong Zheng,[a] Lin Xu[b] and Biao Dong[b]

Ag cluster catalyst-based oxidation of CO to $CO_2$ is an important way to remove CO at low temperatures. However, the instability of silver clusters seriously limits the catalytic application. Herein, sub-nanosized EMT zeolite nanoparticles served as Ag cluster carriers with high selectivity, low coordination, and unsaturated atom active sites. The silver clusters with sub-nanometer size can be controlled with different charge states and loading rates. A detection film with 500 nm was further prepared by assembling the Ag-EMT composites with a small amount of Nalco as an adhesive. For CO detection, a completely enclosed gas sensing device based on *in situ* infrared spectroscopy was employed without air interference. CO was accurately introduced into the detection chamber and catalysed into $CO_2$ by silver loaded EMT zeolite films, and the whole process was accurately recorded by infrared spectroscopy. CO with a detection range of 2–50 ppm was realized, showing great application potential in gas monitoring.

Received 14th April 2023
Accepted 5th June 2023

DOI: 10.1039/d3na00238a

rsc.li/nanoscale-advances



## Introduction

Carbon monoxide, as a colorless, tasteless, and highly flammable gas, is one of the key pollutants in the natural atmosphere and indoor environment. In addition, even at a low concentration of 30 ppm, CO can be highly compatible with human hemoglobin, causing dizziness, vomiting, shock, and other related toxic symptoms.[1–3] The data from World Health Organization showed that one can tolerate 9 μL $L^{-1}$ CO within 8 h and 26 μL $L^{-1}$ within 1 h. Unfortunately, in addition to this, the gas can threaten human life. Based on this situation, there are various CO gas sensors to monitor CO. However, because of the high-risk index of combustible gas detected by conventional catalysts at high temperatures, it is necessary to prepare a highly sensitive sensor for real-time CO monitoring at room temperature.[4,5] Catalytic oxidation of CO to $CO_2$ at low temperatures is a common way of removing CO for purification and is also important for CO detection.[6,7] The noble metal catalysts containing Au and Pt have been widely used in the catalytic oxidation of CO to $CO_2$ with good performance. Compared to the expensive Au and Pt noble metal,[8–10] supported Ag catalysts which, however, are relatively cheap, show excellent low-temperature activities for CO oxidation.[11] The supports for Ag catalysts have two categories: inert supports, such as silica[12,13] and $Al_2O_3$ (ref. 14 and 15) and active supports, such as $CeO_2$,[16–18] $FeO_x$,[19–21] $CoO_x$[22] and $TiO_2$.[23] As alternatives to oxide supports, graphite[24] and carbon nanotubes[25] have also been employed. Generally, in such systems, silver particles should be dispersed finely with a high surface/volume ratio for efficient use. However, due to the very high reactivity, the above-mentioned supports and preparation methods always show bad control for the dispersion of silver particles with a small size, especially the sub-nanometer. Note that recent theoretical and experimental results demonstrated that sub-nanometer clusters have better catalytic activity and/or selectivity than nanometer-sized particles[26–31] because of low co-ordination, unsaturated atoms often function as active sites, and, therefore, downsizing the silver to sub-nanometer particles or clusters is highly desirable for the applications.

Zeolites are perfectly suited to accommodate oligoatomic metal clusters due to their molecularly sized cages and channels, and silver nanoparticles (NPs) can normally be embedded with ship-in-a-bottle confinement strategies.[32–34] In addition, besides the matrix function, the versatile microporous molecular sieves and especially zeolite with respect to pore structure, surface area, catalytic activity, particle dimensions, and morphology are of particular interest for chemical sensor and membrane applications.

In the case of catalytic oxidation and chemical sensors toward CO at room temperature (RT), a number of investigations on interactions of silver zeolites with carbon monoxide have also appeared in the literature since 1990s. G. Caizaferri *et al.*[35] found the fast and stable co-ordination of CO on $Ag^+$-A

[a]*Department of Cell Biology, College of Basic Medical Science, Jilin University, China. E-mail: jiaosun@jlu.edu.cn*

[b]*State Key Laboratory on Integrated Optoelectronics, College of Electronic Science and Engineering, Jilin University, China*

† Electronic supplementary information (ESI) available. See DOI: https://doi.org/10.1039/d3na00238a

‡ Yuda Wang and Haitao He contributed equally to this work.

zeolite together with the potential to oxidize CO to $CO_2$ completely by adding an optimized amount of water, which could be used for the purification of gases. Water plays a key function in this process. It was also found that $Ag^+$ on Ag-NaY catalyst was very important for the enhancement of CO oxygen activity at low temperatures in the range of 55–70 °C,[36] while the exact oxidation process is still a matter of debate. A detailed understanding of this involved process is significant since such small and stabilized Ag clusters, especially when confined in zeolite hosts with excellent stability, having interesting, but so far not well understood, catalytic property.

The motivation for the present work rests on the controlled synthesis of silver cluster loaded nanosized EMT zeolites with different charge states and loading amounts and further assembly in thin films for the detection of carbon monoxide at room temperature (RT). In the preparation process, a small amount of Nalco was employed as a binder, which also can provide the hydroxy groups and play a similar role as water in G. Caizaferri's work.[35] Based on the catalytic oxidation property of the Ag-loaded EMT zeolite films, the low concentrations of CO can be detected by monitoring the amount of $CO_2$ by *in situ* IR spectroscopy.

# Experimental section

### Synthesis of silver-EMT zeolites

A template-free $Na_2O$–$Al_2O_3$–$SiO_2$–$H_2O$ precursor system was employed for the preparation of the nanosized EMT-type zeolite as follows: solution A was prepared by dissolving 9.074 g of sodium aluminate (Strem Chemicals, 56.2% $Al_2O_3$, 39.5% $Na_2O$) and 1.61 g of sodium hydroxide (Prolabo, 97%) in 100 g of distilled water followed by mixing with 44.00 g of sodium hydroxide to give a clear suspension; solution B was prepared by adding 57.692 g of sodium silicate (Prolabo, 27% $SiO_2$, 8% $Na_2O$) and 20.00 g of sodium hydroxide in a 250 ml bottle containing 80 g of distilled water, followed by stirring until the solution became completely transparent. Both solutions were cooled in an ice bath (277 K). Then, solution A was poured slowly into solution B under vigorous stirring. A suspension was formed with the following molar composition: $18.45Na_2O : 1Al_2O_3 : 5.15SiO_2 : 240H_2O$. The suspension was continuously stirred for 5 min, and then kept at 35 °C for 36 h. The zeolite samples were collected and purified to pH 8.

The EMT zeolite formed stable colloidal suspensions and the silver ion exchange was performed in an aqueous medium to avoid agglomeration. The ion-exchange process was performed as follows: 20 ml silver perchlorate solutions with a concentration of 0.05 M were added to three dispersed EMT zeolite suspensions (7.5 wt%, 12 ml) and kept for 2 h and 6 h. The ion-exchanged samples were purified three times *via* high-speed centrifugation and redispersed in water. The reduction of silver cations to nanoparticles (Ag NPs) in the EMT zeolite suspensions (2 wt%, 7 ml) was obtained under microwave reduction (120 °C, 10 min, 1000 W, Anton Paar Synthos 3000) in the presence of triethylamine as reducing agent ($N(C_2H_5)_3$, 0.5 ml, 2 ml, and 4 ml). The reduced suspensions were again purified three times and finally dispersed in water. For clarity, the samples with different ion exchange times can be divided as $Ag^+$-EMT-1 (ion exchange time: 2 h) and $Ag^+$-EMT-2 (ion exchange time: 6 h). After reduction with an increasing amount of reducing agent ($N(C_2H_5)_3$, 0.5 ml, 2 ml, and 4 ml), the samples can be abbreviated as Ag-EMT-1a (0.5 ml $N(C_2H_5)_3$), Ag-EMT-1b (2 ml $N(C_2H_5)_3$), Ag-EMT-1c (4 ml $N(C_2H_5)_3$), Ag-EMT-2a (0.5 ml $N(C_2H_5)_3$), Ag-EMT-2b (2 ml $N(C_2H_5)_3$), and Ag-EMT-2c (4 ml $N(C_2H_5)_3$).

### Synthesis of silver-EMT films

The Ag-EMT suspensions were assembled in thin films with the binder of Nalco on silicon wafers by the spin-coating method. 2 drops of Nalco (2326, silica as $SiO_2$: 15%) served as a binder and were added into 1.6 ml Ag-EMT suspension with a solid content of 0.3 wt% under sonic.

The silicon wafers (100) were precleaned with ethanol and acetone prior deposition of the films. To ensure the preparation of smooth and homogeneous films, the Ag-EMT coating suspensions were filtrated through syringe filters (450 nm), and the spin coating procedure (acceleration: 5000 rpm $s^{-1}$, 5000 rpm for 180 s) was repeated 5 times (each coating step uses three drops of suspension, after which the films were dried at 90 °C for 30 min). The final films have a thickness of 500 nm and cover entirely the silicon wafers with a dimension of 10 × 10 $mm^2$.

### Characterisation of samples

The size and confinement arrangements of Ag within the zeolite nanocrystals were determined by transmission electron microscopy (TEM) using a FEI Titan 80–300 operating at 300 kV. The presence of silver in zeolite was confirmed by the energy-dispersive X-ray spectrometry-transmission electron microscopy (EDX-TEM). The size of Ag-EMT crystals in the coating suspensions was also determined with dynamic light scattering (DLS) using a Malvern Zetasizer-Nano instrument equipped with a 4 mW He–Ne laser (633 nm). The chemical composition of the samples was measured on a Varian Vista AX CCD inductively coupled plasma atomic emission spectrometer (ICP-AES). UV-vis absorption spectra of the silver loaded zeolite suspensions were recorded using a Varian Cary 4000 spectrophotometer. The Ag-EMT type films were characterized by scanning electron microscopy (SEM) using a Philips XL30 FEG. The feature of the films was measured by atomic force microscope (AFM, Innova, Brüker) and analyzed in tapping mode at ambient conditions with a 512 pixels lateral resolution. SNL tips ($k$ ~0.24 N $m^{-1}$, tip radius ~2 nm; Brüker) with a resonant frequency of 54.7 kHz were used, and a slight decrease in set-point of about 0.5 V was necessary for image stability and low streaking. A scan frequency of 0.5 Hz was used.

### *In situ* IR detection of carbon monoxide with Ag-EMT zeolite films

The molecular detection with Ag-containing zeolite films is followed by *in situ* IR spectroscopy, and the experimental setup is shown in (Fig. 1). It is composed of a sample compartment (IR reactor cell) and a gas flow system. The IR reactor cell consists of

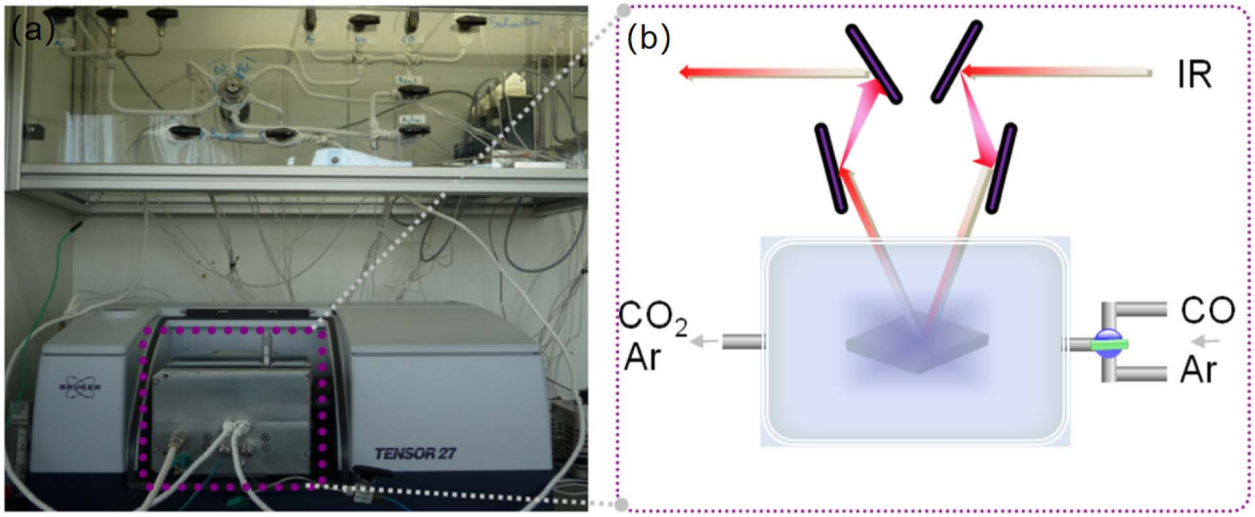


Fig. 1 (a) The experimental setup for CO sensing with a gas flow system and *in situ* IR reactor cell. (b) Scheme of the *in situ* IR system for detection of CO with Ag-containing zeolite films.

a modified diffuse IR cell (diffuse reflectance accessory, Pike) and an environmental chamber for the study of supported films under controlled flow and temperature. The IR reactor cell is equipped with a heating system working at temperatures up to 300 °C, while an air-cooling system is used to protect both the KBr windows and the Viton o-rings. All experiments were carried out at atmospheric pressure. The gases were introduced *via* a saturator using the corresponding Antoine's coefficients to calculate the correct flow and temperature values.

The two gases (mixed gas of Ar and CO and pure Ar) were sent independently to the IR reactor cell. The gas compositions used for the experiments are as follows: activation flow, Ar with a total flow of 25 $cm^3$ $min^{-1}$; reaction flow, CO with a concentration of 2–50 ppm, diluted in Ar with a total flow of 20 $cm^3$ $min^{-1}$. The ZnO/$SnSe_2$ sensor developed by Wang *et al.*[4,5] had the maximum response in the CO concentration range of 10–1000 ppm, with a maximum response of 200 ppm CO. *In situ* IR molecular detections of a single gas or mixtures were carried out at 25 °C. The IR spectra were collected in a continuous mode (64 scans per spectrum) with a Tensor[37] spectrometer (Bruker) equipped with a DTGS detector.

## Results and discussion

### General characterization of Ag-EMT samples

The particle size and shape of the Ag-containing nanosized crystals in the coating suspensions prior to film deposition are studied by TEM, as shown in (Fig. 2). The TEM images of Ag-EMT-1b and Ag-EMT-2b coating suspensions reveal that the size of the individual crystalline particles is about 20 nm, and the crystalline fringe characteristics for the EMT type of structure are visible (Fig. 2a and b). While in the samples Ag-EMT-2b (Fig. 2b), with long-time ion exchange, the amount of silver is considerably increased, which leads to partial leaking from the zeolite matrix to form bigger Ag NPs with a size of 2–5 nm, and in all cases, they are strongly attached and accessible.

The different amounts of loaded silver can also be proved by the TG measurements. The weight loss curve of TG results before 250 °C corresponds to the water inside the supercages, which stabilizes the silver ions. It can be seen that the water content of pure EMT and silver containing EMT samples also decrease with the increase in silver amount (Fig. 2c).

Sub-nanometer sized silver clusters in Ag-EMT zeolite can be recorded by TEM measurement on the cupper grid. From the enlarged images of the sample, extremely small spots having a higher contrast than the zeolite, possibly related to the presence of confined silver clusters, are exclusively detected inside the sodalite cages of the EMT nanocrystals (Fig. 2d). To investigate the position of the silver clusters, the schematic diagram of EMT framework structure was overlapped with the TEM images, and the results show a good match and the silver clusters (black dots) stay separately in the sodalite cages.

The XPS results of the synthesized nanozeolite are shown in Table 1. From the surface analysis, the Si/Al, Ag/Al, and Na/Al ratios are similar between the reduced and unreduced samples. It means the microwave reduction did not cause the silver loss in the crystal growth process.

The particle size and stability of the Ag-containing nanosized crystals in the coating suspensions prior to film deposition are studied by DLS. The sizes of the Ag-EMT nanoparticles (NPs) with different silver concentrations were measured to be about 50 ± 5 nm, as shown in Fig. 3a and b. The result is slightly bigger than that determined with TEM, which could be explained by the dynamic interactions between the zeolite nanoparticles, their surface structure, concentration, and ions present in the dispersion medium. The ζ potential value using the Huckel equation for all the samples is about −40 mV, which corresponds to stable colloidal suspensions. Irreversible agglomeration of the crystalline Ag-EMT nanoparticles in the suspensions was not observed for a period of 24 months; *i.e.*, no change of ζ potential value was found for this period. The previously reported pd-modified $WSe_2$ (Pd–$WSe_2$) nanosheet

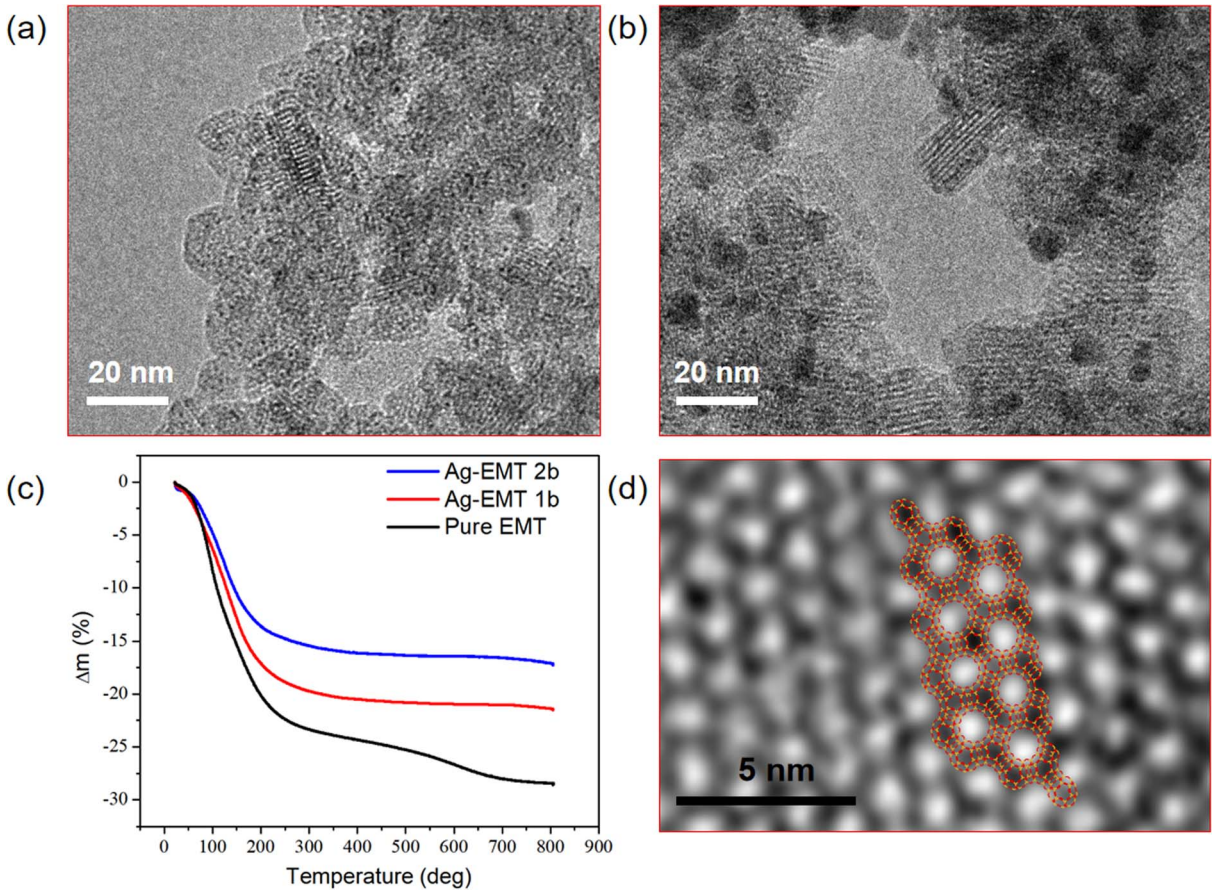


Fig. 2 TEM images of (a) Ag-EMT 1b and (b) Ag-EMT 2b and (insets) corresponding EDX analysis. (c) TG curves of pure EMT, $Ag^0$-EMT 1b, and $Ag^0$-EMT 2b samples. (d) Enlarged TEM images of Ag-EMT zeolite and the schematic diagram of EMT framework structure.

Table 1 XPS results of $Ag^+$-EMT and $Ag^0$-EMT samples

| Sample | Si/Al | Ag/Al | Na/Al |
|---|---|---|---|
| $Ag^+$-EMT-1 | 1.24 | 0.22 | 0.56 |
| $Ag^0$-EMT-1b | 1.25 | 0.24 | 0.62 |
| $Ag^+$-EMT-2 | 1.25 | 0.63 | 0.24 |
| $Ag^0$-EMT-2b | 1.16 | 0.64 | 0.21 |

sensors and ZnO/$SnSe_2$ composite film sensors developed by Wang *et al.*[4,5] were exposed to different concentrations of CO gas with no significant change in the percentage response over 30 days, which also confirms its good long-term stability. Though naked silver clusters are not stable in the solution, they can be well protected with the zeolite channels. To further prove the great colloidal stability of Ag-EMT NPs, the colloidal solution (before and after reduction) was placed in an oven, and then the zeolites became aligned wires during the water evaporation process, indicating that the zeolite nanocrystals have always been in a colloidal state and slowly aligned as wires with evaporation (Fig. S1†).

The stable Ag-EMT suspensions were spin-coated on thin films on the silicon wafers. The samples have the same thickness since they pass the same spin-coating procedure. Side and top views of $Ag^0$-EMT-1b (Fig. 3c) and $Ag^0$-EMT-2b (Fig. 3d) by SEM and AFM measurements are selected as examples. The zeolite crystals are well-packed and form dense and homogeneous films with an ultimate thickness of about 500 nm. The surface feature from AFM measurements confirms the flat morphology of the films. The size of the embedded particles is estimated to be 20–30 nm, in good agreement with TEM measurements.

### *In situ* IR detection of carbon monoxide with Ag-EMT films

The as-prepared Ag-EMT films on silicon wafers (500 nm in thickness) are exposed to the mixture of CO and Ar. The gas mixtures are sent independently to the IR reactor cell containing the films, and the spectra are collected continuously. The same experiments were carried out on the pure EMT, $Ag^+$-EMT, and Ag-EMT samples. During the measurements, a constant water concentration of 100 ppm in the cell was measured coming from the carrier gas (argon). The entire process, including the activation of samples (removal of adsorbed water and contaminants) and controlled adsorption and desorption of analytes, was carried out in the IR reactor cell (Fig. 1).

The spectra for the detection of CO on $Ag^0$-EMT-2b film are shown in (Fig. 4a). As can be seen, adding CO to the Ag-EMT sample leads instantaneously to the appearance of a gas

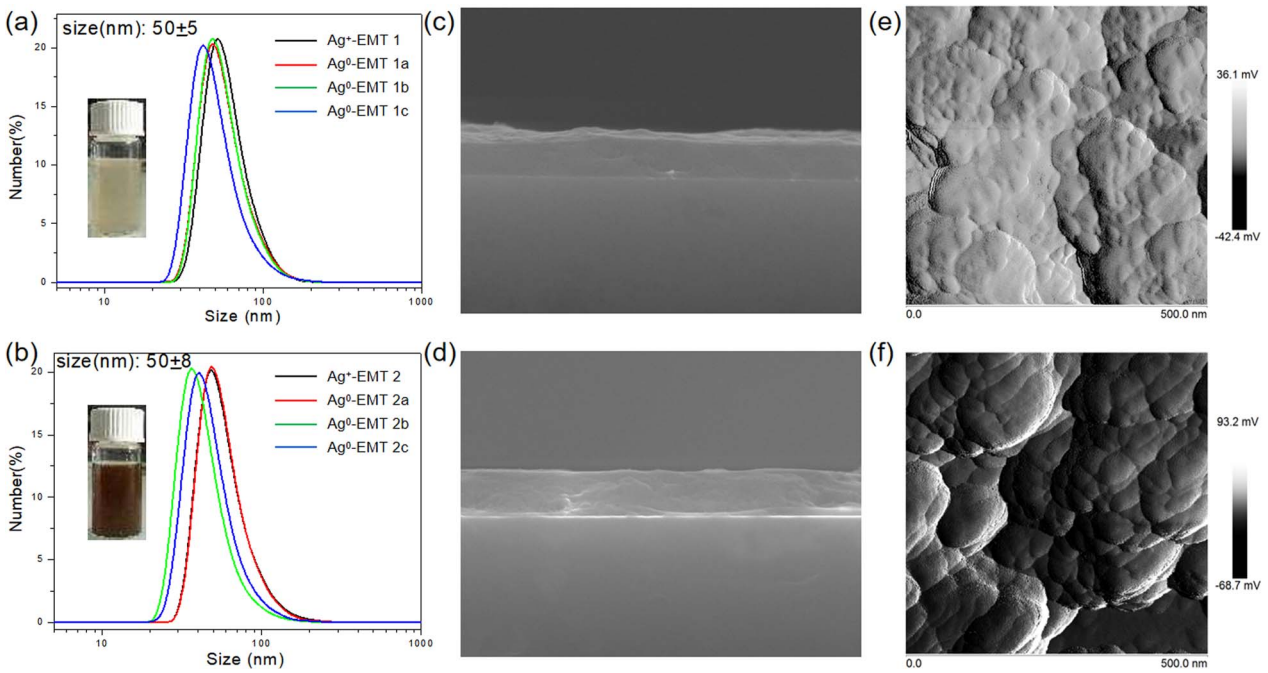


Fig. 3 Particle size distribution curves of the (a) Ag-EMT 1 and (b) Ag-EMT 2 samples. The average size of the nanoparticles is 50 ± 5 nm. The insets are coating suspensions of Ag-EMT 1b and Ag-EMT 2b, respectively. (c) and (d) are the SEM images of Ag-EMT films of Ag-EMT 1b and Ag-EMT 2b, and the thickness is 500 nm. The scale bar is 2 μm. (e) and (f) are the AFM images of the Ag-EMT films of Ag-EMT 1b and Ag-EMT 2b.

phase $CO_2$ band centered at 2236 and 2210 $cm^{-1}$. Meanwhile, the characteristic bands of adsorbed carbon monoxide on the Ag and Al cations in zeolite appear from 2200 to 2275 $cm^{-1}$. Increasing the CO concentration from 2 to 50 ppm at room temperature (RT) resulted in an increased intensity of $CO_2$. The intensities of $CO_2$ dependent on the amount of CO were plotted (Fig. 4b). As can be seen, the intensity of the $CO_2$ band increases in both silver containing films, but no $CO_2$ signal was observed for the pure EMT films. In $Ag^0$-EMT-2b film, a liner trend dependent on the CO concentration can be found before 35 ppm and then the saturation is reached. However, for Ag-EMT-1b film, no saturation appears in the range of 2–50 ppm, but the intensity is lower than that with a higher amount of silver. In the case of CO sensing, it is very important for the detection in this range since human health can be harmed by CO with more than 30 ppm.[37]

Considering that the optical path in the IR machine was filled with nitrogen, the detected $CO_2$ should be in the cell and comes from the transformation of oxidized CO. Note that the size of the individual zeolite nanocrystals and the thickness of

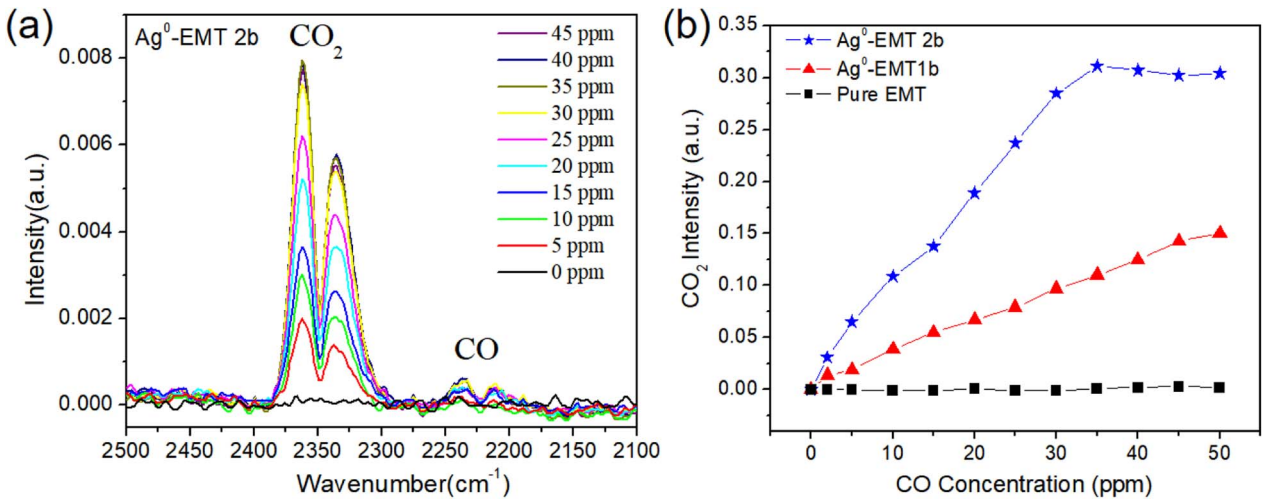


Fig. 4 (a) *In situ* IR spectra Ag-EMT-2b film by increasing the CO concentration from 2 to 50 ppm at RT. (b) The IR absorption intensities of $CO_2$ dependent on the amount of CO with pure EMT, Ag-EMT-1b, and Ag-EMT-2b films in the range of 2–50 ppm.

the films are comparable, while the silver contents in samples are 0 wt%, 9 wt%, and 18 wt% from ICP analysis, respectively, which is also in good accordance with the changes of the $CO_2$ intensity. Therefore, the silver inside the zeolite plays a key role in the catalytic oxidation of CO.

Since there is no oxygen gas in the system, some oxygen species should exist in the film. Normally, water can be involved in the oxidation of CO to $CO_2$ from the results of G. Caizaferri *et al.*[35] In this work, we suppose that the binder Nalco plays a similar role to water since it has much more hydroxyl groups besides the function of crosslinker. It is also confirmed by the same experiment with the film of Ag–zeolite without Nalco binder, which shows no $CO_2$ signal (Fig. S2†). Considering the reaction in the results of G. Caizaferri *et al.*,[35] we propose a possible reaction with the following equation: $6Si{-}OH + CO + 2Ag^{+} \rightarrow 2Ag^{0} + CO_2 + 3Si{-}O{-}Si + 2H_3{}^{+}O$, which is catalyzed by silver clusters in the zeolite. $[EMT]\text{-}Ag^{+}\text{-}[CO(OH)]^{-}$ radical can be supposed as a hypothetical intermediate in the reaction.[33]

To elucidate further on this point, the $CO_2$ intensities dependent on CO with $Ag^{+}$-EMT and Ag-EMT samples were carried out, as shown in (Fig. 5a and b). In both cases, only weak bands of $CO_2$ were found in high concentrations of CO for unreduced $Ag^{+}$-EMT samples. As the reducing agent increases, more and more silver cations are reduced to silver NPs, while the $CO_2$ intensity dependent on CO shows an opposite trend in both cases. Among Ag-EMT-2a, 2b, and 2c samples (Fig. 5c and d), the $CO_2$ intensity increases with the increase of the silver metal amount, which indicates that more silver metal promoted the catalytic oxidation of CO. While in the sample of Ag-EMT 1a, 1b and 1c, increasing the reducing agent causes a much slower reaction. Considering the above supposed reaction, these results further confirm that both silver cations and silver NPs are involved in the catalytic oxidation, and serve as reactant and catalyst, respectively. The total amount of silver in EMT zeolite is certain after the ion exchange. Therefore, in Ag-EMT 1a, b, c samples, the reaction speed depends very much on the amount of silver cations, which will be less and less in the reducing environment. While in the sample Ag-EMT 2a, b, c, there are enough silver cations in the EMT zeolite due to the long-time ion exchange even with high amounts of reducing agent. Therefore, more amount of silver metal can serve as a catalyst and control the oxidation behavior.

Comparing the two $Ag^{+}$-EMT samples, both of them show no reaction activity as the CO concentration is low. As the CO amount increases, $Ag^{+}$-EMT-2 shows a little more reactivity relative to $Ag^{+}$-EMT-1, while it is still much lower relative to the

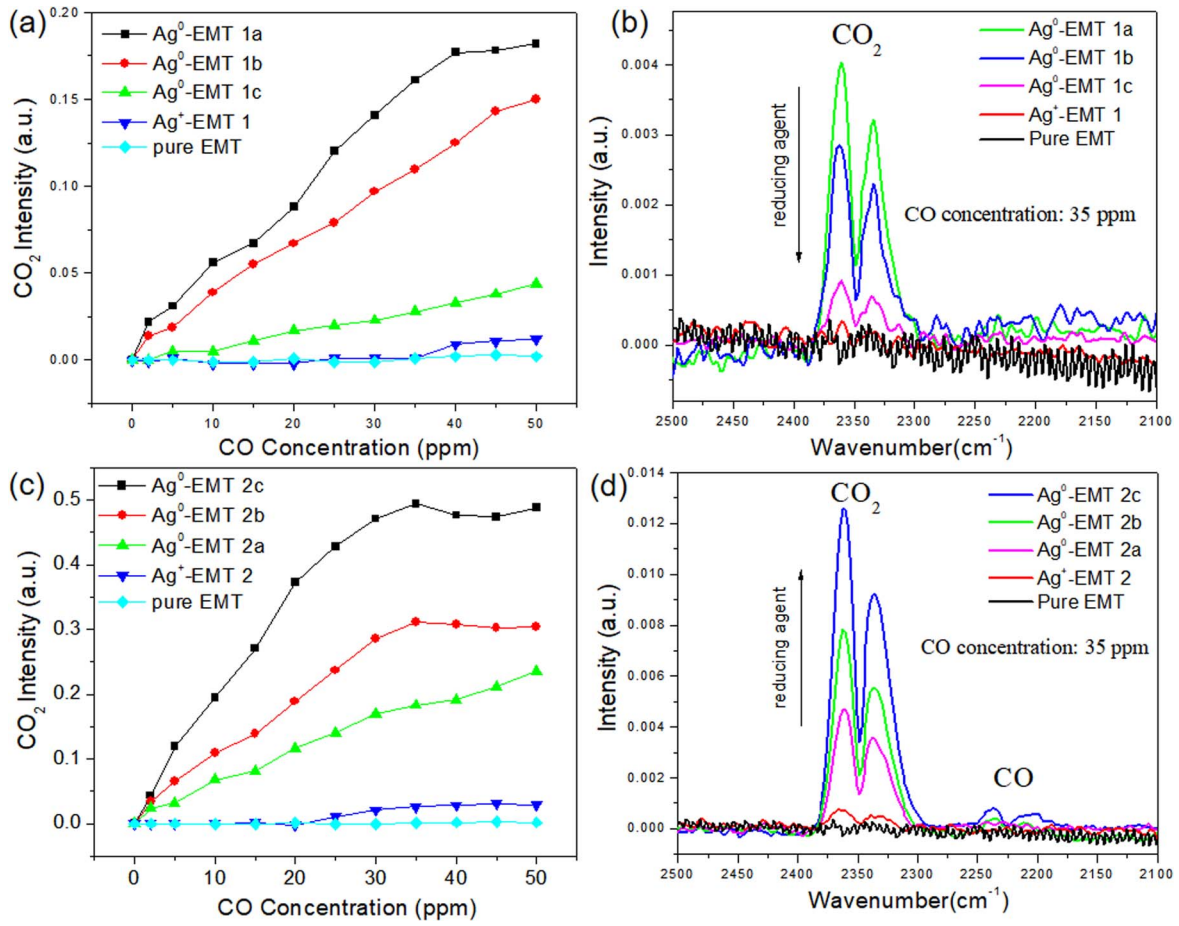


Fig. 5 (a) The $CO_2$ intensities dependent on CO with unreduced $Ag^{+}$-EMT 1 sample and reduced Ag-EMT 1a, 1b, and 1c samples with different amounts of reducing agent and (b) the corresponding *in situ* IR spectra measured. (c) The $CO_2$ intensities dependent on CO with unreduced $Ag^{+}$-EMT 2 sample and reduced Ag-EMT 2a, 2b, and 2c samples and (d) the corresponding *in situ* IR spectra measured.

reduced samples. On the other hand, the weak signal from $Ag^+$-EMT-1 and $Ag^+$-EMT-2 can also suggest that a small amount of silver NPs existed inside the zeolites, which should have formed in the film preparation (spin-coating) process since evaporation of the solvent can also cause the reduction of a small amount of silver. The phenomenon of evaporation of Ag-EMT suspensions in glass bottles can further prove this, as shown in (Fig. S2†). The above results indicate that the condition for the reaction is that Ag cations and Ag NPs are available simultaneously.

The Ag NPs with the sub-nanometer size or clusters are saturated in the sodalite cages, which is proved by the TEM measurements. The hard template effect of zeolite makes the Ag NPs very stable as well as accessible due to the molecular sieve property. Though CO cannot enter the sodalite cage because of its size, catalytic oxidation still happens inside the zeolite in the presence of OH groups and silver cations.

## Conclusions

The preparation of Ag-EMT nanosized zeolite particles by microwave reduction in colloidal suspensions is reported. The current approach permits the preparation of Ag NPs with sub-nanometer size and confined within the sodalite cages of EMT zeolite without agglomeration. The exact position of the metal in zeolite is not easy to confirm, while in this case, EMT nano-zeolites were prepared *via* a template-free method at low temperature and therefore a large loading amount of silver was achieved and monitored by TEM measurements. The stable Ag-containing EMT zeolite suspensions were deposited in thin films with a thickness of 500 nm and further used for the detection of low concentrations of carbon monoxide (2–50 ppm). The detection of CO was carried out with an *in situ* IR system by monitoring the amount of $CO_2$ due to the catalytic oxidation by Ag-EMT at RT. Besides the presence of Ag cations and NPs, Nalco also plays a key role in the reaction. Ag-EMT zeolite film owns the potential to oxidize CO to $CO_2$ completely and could be used for the fast detection of CO, especially on a scale that concerns human health.

## Author contributions

Jiao Sun: idea conception, preparation, data analysis, writing. Yuda Wang: data analysis, writing. Xinyao Zhang: reviewing and editing. Ling Huang: reviewing and editing. Mahmut Zulpya: writing and editing. Haitao He: measurement, Xianhong Zheng: data analysis, Lin Xu: review and editing. Biao Dong: data analysis, editing, reviewing.

## Conflicts of interest

The authors declare no competing financial interest.

## Acknowledgements

This work was supported by the National Natural Science Foundation of China (grant no. 52250077, 52272080, 82073475), the Natural Science Foundation of Jilin Province (20210401059YY, 20220402005GH).

## Notes and references

1 J. A. Rauba, M. Mathieu-Nolfb, N. B. Hampsonc and S. R. Thomd, *Toxicology*, 2000, **145**, 1–14.
2 J. Y. Han, F. F. Han, J. Ouyang, L. X. He, Y. T. Zhang and N. Na, *Nanoscale*, 2014, **6**, 3069–3072.
3 S. R. Thom, D. Fisher, Y. A. Xu, K. Notarfrancesco and H. Ischiropoulos, *Proc. Natl. Acad. Sci. U. S. A.*, 2000, **97**, 1305–1310.
4 D. Z. Zhang, D. Y. Wang, W. J. Pan, M. C. Tang and H. Zhang, *Sens. Actuators, B*, 2022, **360**, 131634.
5 D. Y. Wang, D. Z. Zhang, Q. N. Pan, T. Wang and F. J. Chen, *Sens. Actuators, B*, 2022, **371**, 132481.
6 F. X. Liang, H. Q. Zhu, Z. F. Qin, G. F. Wang and J. G. Wang, *Prog. Chem.*, 2008, **20**, 1453–1464.
7 L. S. Qin, D. H. Yin, J. F. Liu and C. Y. Li, *Chin. J. Catal.*, 2015, **26**, 714–718.
8 D. Zhang, C. Z. Zhang, D. B. Mu, B. R. Wu and F. Wu, *Acta Chim. Sin.*, 2013, **71**, 1101–1110.
9 R. R. Hu, Y. Cheng, L. Y. Xie and D. Z. Wang, *Chin. J. Catal.*, 2007, **28**, 463–468.
10 C. R. Song, Q. F. Ge and L. C. Wang, *J. Phys. Chem. B*, 2005, **109**, 22341–22350.
11 C. H. Tu, A. Q. Wang, M. Y. Zheng, Y. Meng, J. H. Shan and T. Zhang, *Chin. J. Catal.*, 2005, **26**, 631–633.
12 H. Y. Liu, D. Ma, R. A. Blackley, W. Z. Zhou and X. H. Bao, *Chem. Commun.*, 2008, 2677–2679.
13 J. C. Zheng, J. Liu, W. Wei and Q. Sun, *Chin. J. Catal.*, 2008, **29**, 1199–1201.
14 J. Wang, R. You, K. Qian, Y. Pan, J. Z. Yang and W. X. Huang, *Chin. J. Catal.*, 2021, **42**, 2242–2253.
15 Y. J. Mu, C. M. Geng, M. Z. Wang, H. Wu, X. S. Zhang and G. B. Jiang, *J. Geophys. Res.: Atmos.*, 2004, **109**, D13301.
16 P. Bera, K. C. Patil and M. S. Hegde, *Phys. Chem. Chem. Phys.*, 2000, **2**, 3715.
17 R. C. Rao, H. W. Liang, C. M. Hu, H. Z. Dong, X. Z. Dong, Y. Q. Tang, S. Fang and Q. Ling, *Fuel*, 2022, **317**, 123439.
18 G. D. Li and Z. Y. Tang, *Nanoscale*, 2014, **6**, 3995.
19 K. M. Jia, H. L. Zhang and W. C. Li, *Chin. J. Catal.*, 2008, **29**, 1089–1092.
20 M. Chen and X. M. Zheng, *Environ. Chem.*, 2000, **19**, 110.
21 Z. Y. Pan, H. Li, Y. X. Qiao, H. M. Yang, X. G. Zhao, B. Feng, W. W. Zhu and Z. S. Hou, *Chin. J. Catal.*, 2011, **32**, 428–435.
22 S. Y. Zhang, J. J. Zhan, H. Zhou, M. S. Niu, H. H. Yang, X. Zhou, X. L. Yi and Y. Liu, *Jece*, 2022, **10**, 108844.
23 N. Comsup, J. Panpranot and P. Praserthdam, *Catal. Commun.*, 2010, **11**, 1238.
24 D. C. Lim, I. Lopez Salido and Y. D. Kim, *Surf. Sci.*, 2005, **598**, 96.
25 Y. M. Dai, T. C. Pan, W. J. Liu and J. M. Jehng, *Appl. Catal., B*, 2011, **103**, 221.
26 A. A. Herzing, C. J. Kiely, A. F. Carley, P. Landon and G. J. Hutchings, *Science*, 2008, **321**, 1331–1335.

27 M. Turner, V. B. Golovko, O. P. H. Vaughan, P. Abdulkin, A. Berenguer-Murcia, M. S. Tikhov, B. F. G. Johnson and R. M. Lambert, *Nature*, 2008, **454**, 981–983.
28 S. Vajda, J. Pellin Michael, P. Greeley Jeffrey, L. Marshall Christopher, A. Curtiss Larry, A. Ballentine Gregory, W. Elam Jeffrey, C.-M. Stephanie, C. Redfern Paul, M. Faisal and Z. Peter, *Nat. Mater.*, 2009, **8**, 213–216.
29 K. Judai, S. Abbet, A. S. Worz, U. Heiz and C. R. Henry, *J. Am. Chem. Soc.*, 2004, **126**, 2732–2737.
30 Y. Lei, F. Mehmood, S. Lee, J. Greeley, B. Lee, S. Seifert, R. E. Winans, J. W. Elam, R. J. Meyer, P. C. Redfern, D. Teschner, R. Schlögl, M. J. Pellin, L. A. Curtiss and S. Vajda, *Science*, 2010, **328**, 224–228.
31 Z. Chen, Y. Liang, D. S. Jia, Z. M. Cui and W. G. Song, *Chin. J. Catal.*, 2017, **38**, 651–657.
32 E. Koohsaryan and M. Anbia, *Chin. J. Catal.*, 2016, **37**, 447–467.
33 J. F. Li, K. Zhang, N. Wang and Q. M. Sun, *Chem. J. Chin. Univ.*, 2022, **43**, 20220032.
34 Q. R. Li, X. L. Tian, J. P. Yuan, D. Zhao, Y. G. Wang and H. R. Li, *Inorg. Chem.*, 2023, **62**, 2430–2439.
35 G. Caizaferri, W. Suter and B. Waldeck, *J. Chem. Soc., Chem. Commun.*, 1990, 485–487.
36 H. Xiao, J. Zhang, J. Dong, M. Luo, R. Lee and V. Romero, *Opt. Lett.*, 2005, **30**, 1270.
37 R. D. Stewart, *J. Occup. Med.*, 1976, **18**, 304–309.